

Gravitational-wave spin-down and stalling lower limits on the electrical resistivity of the accreted mountain in a millisecond pulsar

M. Vigeliu¹ and A. Melatos¹

`mvigeliu@physics.unimelb.edu.au`

Received _____; accepted _____

¹School of Physics, University of Melbourne, Parkville, VIC 3010, Australia

ABSTRACT

The electrical resistivity of the accreted mountain in a millisecond pulsar is limited by the observed spin-down rate of binary radio millisecond pulsars (BRMSPs) and the spins and X-ray fluxes of accreting millisecond pulsars (AMSPs). We find $\eta \geq 10^{-28} \text{ s } (\tau_{\text{SD}}/1 \text{ Gyr})^{-0.8}$ (where τ_{SD} is the spin-down age) for BRMSPs and $\eta \geq 10^{-25} \text{ s } (\dot{M}_a/\dot{M}_E)^{0.6}$ (where \dot{M}_a and \dot{M}_E are the actual and Eddington accretion rates) for AMSPs. These limits are inferred assuming that the mountain attains a steady state, where matter diffuses resistively across magnetic flux surfaces but is replenished at an equal rate by infalling material. The mountain then relaxes further resistively after accretion ceases. The BRMSP spin-down limit approaches the theoretical electron-impurity resistivity at temperatures $\gtrsim 10^5 \text{ K}$ for an impurity concentration of ~ 0.1 , while the AMSP stalling limit falls two orders of magnitude below the theoretical electron-phonon resistivity for temperatures above 10^8 K . Hence BRMSP observations are already challenging theoretical resistivity calculations in a useful way. Next-generation gravitational-wave interferometers will constrain η at a level that will be competitive with electromagnetic observations.

Subject headings: accretion, accretion disks – stars: magnetic fields – stars: neutron – pulsars: general.

1. Introduction

Recent searches for periodic gravitational wave signals from isolated (Abbott et al. 2007b; Wette et al. 2008; Abbott et al. 2008) and accreting (Abbott 2007b; Watts et al. 2008) neutron stars with the Laser Interferometer Gravitational Wave Observatory (LIGO) have placed new upper limits on the mass quadrupole moments of these objects. In rare instances, the LIGO upper limit beats the indirect limit inferred from electromagnetic spin-down observations, e.g. the Crab’s mass ellipticity is measured by LIGO to be $\epsilon \leq 1.8 \times 10^{-4}$, approximately 25% of the indirect limit (Abbott et al. 2008). More often, the indirect limit beats the LIGO limit, e.g. for slowly decelerating radio millisecond pulsars (Abbott et al. 2007b).

As theoretical models for the quadrupole become more accurate and sophisticated, spin-down measurements and LIGO nondetections translate into stricter limits on the constitutive properties of a neutron star. For example, the quadrupole produced by electron-capture gradients requires a persistent lateral temperature difference of $\sim 5\%$ at the base of the outer crust, and a normal rather than superfluid core, to be consistent with the gravitational-wave stalling interpretation of low-mass X-ray binary (LMXB) spins (Ushomirsky et al. 2000). The compressibility of nuclear matter must be lower than ~ 200 MeV to explain the nondetection of a gravitational wave signal from large pulsar glitches (van Eysden & Melatos 2008). The breaking strain of the crust is bounded above by the nondetection of a gravitational-wave signal from accreting neutron stars (Haskell et al. 2007; Watts et al. 2008; Horowitz & Kadau 2009).

In this paper, we show how the observed spin-down rates of binary radio millisecond pulsars (BRMSPs), and the spins and X-ray fluxes of accreting millisecond pulsars (AMSPs), translate into lower bounds on the electrical resistivity of an accreted neutron star crust. The bounds arise because the magnetically confined polar mountain formed during

accretion (Payne & Melatos 2004; Melatos & Payne 2005) must relax resistively, until the quadrupole is low enough to respect the observational limits. Such an argument can be mounted now with rising confidence, because there have been substantial improvements recently in our understanding of the structure of magnetic mountains, including studies of ideal-magnetohydrodynamic (ideal-MHD) instabilities (Payne & Melatos 2006; Vigelius & Melatos 2008, 2009a), Ohmic diffusion (Vigelius & Melatos 2009b), realistic equations of state (Priymak & Melatos 2009), and hydrodynamic sinking into the non-rigid crust (Wette et al. 2009). The theory is now robust enough that its prediction of large ideal-MHD quadrupoles ($\epsilon \sim 10^{-5}$) deserves to be taken seriously. One must therefore appeal to nonideal processes, like resistive relaxation, to bring ϵ below $\sim 10^{-8}$, as the observational limits require.

The paper is set out as follows. In §2, magnetic mountain models are briefly reviewed, and an approximate formula is given for ϵ as a function of accreted mass, electrical resistivity, and age. The formula is applied to convert observations of BRMSP spin-down rates (§3) and AMSP spin frequencies (§4) into lower limits on the electrical resistivity, assuming energy conservation and gravitational-wave stalling respectively. In §5, the limits are mapped onto a resistivity-versus-temperature plot and compared with the latest theoretical calculations of the electron-phonon and electron-impurity resistivities (Itoh & Kohyama 1993; Baiko & Yakovlev 1996; Cumming et al. 2001, 2004). The prospect of better limits from future LIGO experiments is canvassed briefly.

2. Magnetic mountain quadrupole

The quadrupole generated by hydromagnetic stresses from the natal magnetic field of a neutron star (before accretion begins) is too small to emit gravitational waves at a level detectable in the spin down of MSPs or by LIGO. For dipolar fields in the range 10^{12} G

$\leq B \leq 10^{13}$ G (Hartman et al. 1997; Arzoumanian et al. 2002; Faucher-Giguère & Kaspi 2006), one obtains $h_0 \lesssim 10^{-30}$ for the gravitational wave strain and $|\dot{f}_*| \lesssim 4 \times 10^{-32}$ Hz s⁻¹ for the frequency spin-down rate (Bonazzola & Gourgoulhon 1996). A stochastic magnetic field in a type I superconducting core, or a strong toroidal field ($\gtrsim 10^{14}$ G), give $h_0 \sim 10^{-27}$ and $|\dot{f}_*| \sim 10^{-25}$ Hz s⁻¹ (Cutler 2002).

On the other hand, magnetic burial by accretion leads to a much larger quadrupole, as accreted material is funneled onto the polar cap. Payne & Melatos (2004) computed the *unique*, quasistatic sequence of ideal-MHD equilibria that describes how burial proceeds as a function of the total accreted mass M_a while self-consistently respecting the flux-freezing constraint¹. They found that the accreted matter is confined at the poles by an equatorial belt of compressed magnetic field anchored in the deep crust (Hameury et al. 1983; Brown & Bildsten 1998; Litwin et al. 2001). The resulting ‘magnetic mountain’ has a substantial quadrupole moment, even after it relaxes hydromagnetically through the undular Parker instability. Expressed as a mass ellipticity ϵ_{MHD} , the final ideal-MHD quadrupole is given by (Payne & Melatos 2004; Melatos & Payne 2005; Payne & Melatos 2006; Vigelius & Melatos 2009a; Wette et al. 2009)

$$\frac{\epsilon_{\text{MHD}}}{2 \times 10^{-7}} = \frac{M_a}{M_c} \left(1 + \frac{M_a}{M_c} \right)^{-1}, \quad (1)$$

with $M_c \approx 2 \times 10^{-5} M_\odot$. Numerical simulations, where a mountain is grown *ab initio* by mass injection, confirm the overall scaling for ϵ_{MHD} [with some extra oscillatory dynamics (Vigelius & Melatos 2009a)].

Magnetic mountains relax resistively on the diffusive time scale, $\tau_d = 8.6 \times 10^7$ yr,

¹Flux-freezing is valid in the crust, down to a depth where carbon ignition occurs in one-dimensional models, but not necessarily in the magnetic belt region, where the field is highly distorted and diffusion proceeds faster.

after accretion switches off (Vigelius & Melatos 2009b). In a BRMSP, resistive relaxation proceeds roughly exponentially, with

$$\epsilon = \epsilon_{\text{MHD}} \exp(-t\tilde{\eta}/\tau_{\text{d}}), \quad (2)$$

where $\tilde{\eta}$ measures the resistivity η in units of 1.3×10^{-27} s, and t is the time elapsed since accretion stops [compare Fig. 1 in Vigelius & Melatos (2009b)]. In an AMSP, where accretion continues today, a steady state is established, where the influx of accreted material into a magnetic flux tube exactly replenishes the efflux due to Ohmic diffusion. The steady state is attained when the diffusion time-scale equals the accretion time-scale. As τ_{d} is directly proportional to η , the corresponding saturation ellipticity scales as (Brown & Bildsten 1998; Vigelius & Melatos 2009a)

$$\epsilon = \min \left(\epsilon_{\text{MHD}}, 5.1 \times 10^{-9} \tilde{\eta}^{-1} \dot{M}_{\text{a}} / \dot{M}_{\text{E}} \right), \quad (3)$$

where \dot{M}_{a} and \dot{M}_{E} are the actual and Eddington accretion rates, respectively.

Mountain relaxation is required by existing data. LMXBs should have been detected by LIGO already, if the quadrupole is as large as Eq. (1) predicts (Vigelius & Melatos 2009a). Yet directed searches have found nothing to date (Abbott 2007b; Abbott et al. 2007a).

In general, the magnetic mountain axis is tilted with respect to the rotation axis. Hence the star precesses², generating gravitational waves at f_* and $2f_*$. The polarized wave strain is written down elsewhere (Zimmermann & Szedenits 1979; Jaranowski et al. 1998; Van Den Broeck 2005; Vigelius & Melatos 2009a). Its characteristic amplitude is

$$h_0 = \frac{16\pi^2 G}{c^4} \frac{\epsilon I_{zz} f_*^2}{D} F(\theta, i), \quad (4)$$

²It is therefore possible in principle to measure independently the quadrupole moment from modulations in X-ray light curves, e.g. in RCW 103 or XTE J1814–338 (Heyl 2002; Chung et al. 2008).

where I_{zz} is the moment of inertia, f_* is the spin frequency, D is the distance to the source, θ is the wobble angle, and i is the inclination angle of the line of sight. For small θ , we have $F(\theta, i) \propto \theta$.

We combine ϵ_{MHD} from Eq. (1) with the resistive decay prescriptions in this section and Eq. (4) to derive limits on η in BRMSPs and AMSPs in §3 and §4 respectively. Ideally, ϵ for both BRMSPs and AMSPs should be estimated by the same method, since every AMSP evolves into a BMRSP (Wijnands & van der Klis 1998; Alpar 2008). But we are prevented from making this connection because two crucial pieces of important information are missing: \dot{M}_a for BRMSPs, and the age of AMSPs.

3. Binary radio millisecond pulsars

3.1. Spin down

If we attribute the loss of angular momentum observed in pulsar timing experiments to gravitational wave emission alone, we can write down a corresponding limit on the gravitational wave strength (Abbott et al. 2007b; Wette et al. 2008),

$$h_{\text{SD}} \leq \left(\frac{5GI_{zz}|\dot{f}|}{2c^3 D^2 f} \right)^{1/2}, \quad (5)$$

which translates to an ellipticity

$$\epsilon_{\text{SD}} \leq 5 \times 10^{-8} \left(\frac{|\dot{f}|}{10^{-16} \text{ Hz s}^{-1}} \right)^{1/2} \left(\frac{f}{100 \text{ Hz}} \right)^{-5/2}, \quad (6)$$

where f is the gravitational wave frequency (assumed here to be $2f_*$), and \dot{f} is its time derivative.

We compare ϵ_{MHD} and ϵ_{SD} for those BRMSPs in the literature, whose M_a has been estimated with the help of binary evolutionary simulations assuming that mass transfer is

Object	f_*	$ \dot{f}_* $	D	M_a
	[Hz]	10^{-16} Hz s $^{-1}$	[kpc]	$[M_\odot]$
B0021–72E	283	78	4.9	0.7
B0655+64	5.11	0.179	0.48	0.003
(B0820+02)	1.16	1.40	1.4	0.02
(B1800–27)	2.99	1.53	3.6	0.6
(B1831–00)	1.92	0.388	5.1	0.8
B1913+16	16.0	24	7.1	0.003
B1953+29	163	7.91	5.4	0.06
J0034–0534	533	14	0.980	0.7
J0218+4232	430	140	5.85	0.7
J0437–4715	174	17	0.150	0.8
J1022+1001	60.0	1.6	0.400	0.03
J1045–4509	134	3.1	3.24	0.7
J1713+0747	219	4.1	1.12	0.7
J2019+2425	254	4.5	0.910	0.7
J2145–0750	62.0	1.15	0.500	0.03
J2229+2643	336	1.6	1.43	0.7
J2317+1439	290	2.0	1.89	0.8

Table 1: Binary radio millisecond pulsars for which M_a has been estimated (van den Heuvel & Bitzaraki 1995).

Eddington-limited and conservative (van den Heuvel & Bitzaraki 1995). The objects in this class are listed in Table 1, together with their spin-down parameters, distances, and M_a values. Typical fractional uncertainties in the quoted M_a are $\lesssim 50\%$ (Wijers 1997), mainly because it is unclear how conservative mass transfer really is (van den Heuvel & Bitzaraki 1995). The spin parameters and distance, inferred from the dispersion measure, are drawn from the Australia Telescope National Facility pulsar database³ (Hobbs et al. 2004). We find that the ideal-MHD ellipticity is higher than the spin-down limit for all but three objects (PSR B0820+02, PSR B1800–27, and PSR B1831–00, in parentheses in Table 1). The latter objects are excluded from the subsequent analysis because they do not translate into limits on η .

Assuming that resistive relaxation reduces ϵ_{MHD} below ϵ_{SD} , and that the time available to do so is the spin-down age at the present epoch, $\tau_{\text{SD}} = -\dot{f}_*/(2\ddot{f}_*)$, we can combine (1), (2), and (6) to get a minimum resistivity η_{min} . The results are presented in Fig. 1, which displays η_{min} as a function of τ_{SD} on a log-log plot for the objects discussed in the previous paragraph (filled squares). A least-squares fit yields $\eta_{\text{min}} = 10^{-27.3\pm 0.8} (\tau_{\text{SD}}/1 \text{ Gyr})^{-0.7\pm 0.1} \text{ s}$, where we omit the single obvious outlier at $\tau_{\text{SD}} = 4.5 \times 10^9 \text{ yr}$ from the fit.

Equation (6) is almost certainly too conservative (Owen 2009). If we assume that the electromagnetic torque exceeds the gravitational-wave torque in BRMSPs by at least the same factor (~ 4.1 times) as in the Crab pulsar, as indicated by the results of the LIGO Crab search (Abbott et al. 2008) (an arbitrary assumption, to be sure, but plausible), then we arrive at a more stringent limit on η . Replacing $|\dot{f}_*|$ by $4|\dot{f}_*|$ in Eq. (5), we find that ϵ_{SD} doubles for all the objects plotted in Fig. 1 (open circles). Fitting the open circles, we obtain $\eta_{\text{min}} = 10^{-27.2\pm 0.6} \text{ s} (\tau_{\text{sd}}/1 \text{ Gyr})^{-0.8\pm 0.2}$

³www.atnf.csiro.au/research/pulsar/psrcat/

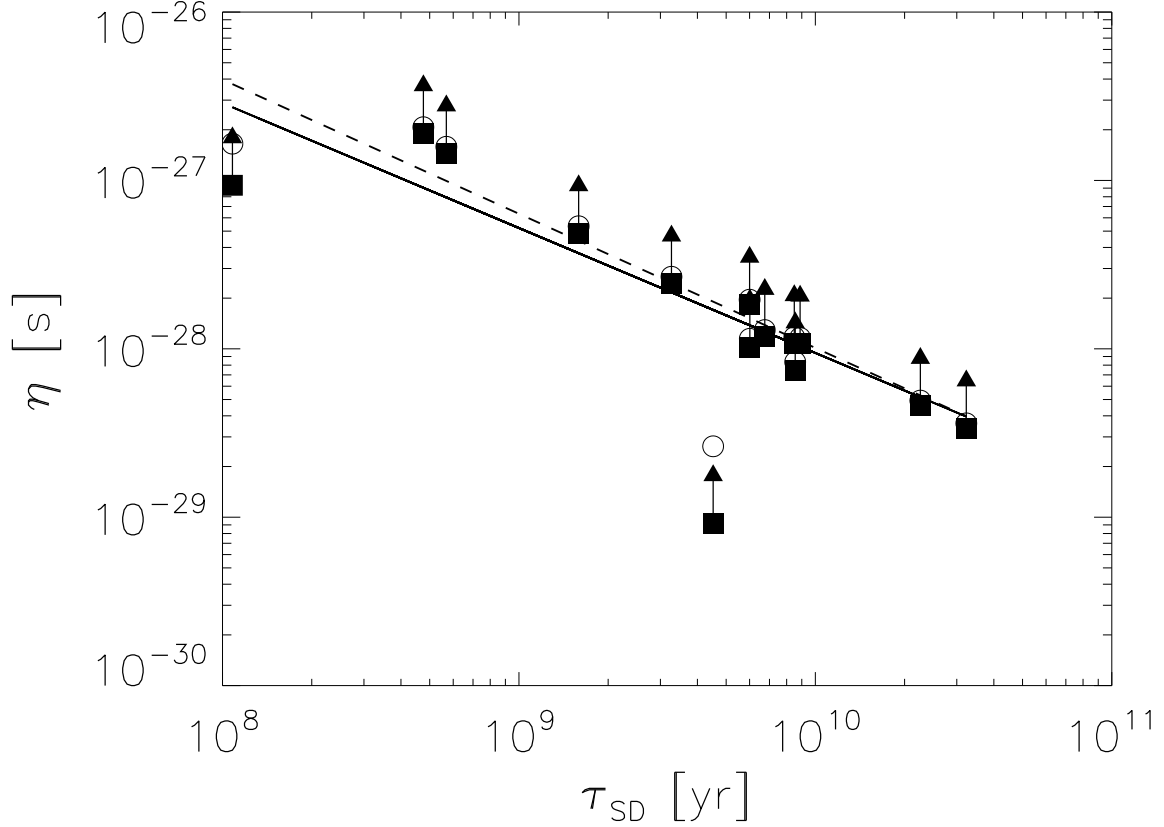


Fig. 1.— Electrical resistivity η (in s), inferred from the spin-down limit for BRMSPs, plotted as a function of characteristic age τ_{SD} (in yr). Lower limits on η from the 14 objects listed in van den Heuvel & Bitzaraki (1995) are shown as filled squares; the three objects with $\epsilon_{MHD} < \epsilon_{SD}$ do not yield useful limits. A more stringent limit on η (open circles) can be obtained by assuming that the electromagnetic torque exceeds the gravitational-wave torque by at least a factor of four, like in the Crab (see text). The solid and dashed lines are power-law fits to the filled squares and the open circles, respectively.

3.2. Nondetection of gravitational waves

In a similar fashion, we can obtain a less stringent lower limit on η from gravitational-wave observations. Directed searches for gravitational waves from known radio pulsars set an upper limit on the wave strain (and hence ϵ) for these objects (Abbott 2007b; Abbott et al. 2007a). We then apply the same argument as in §3.1.

Fig. 2 displays the expected gravitational wave strain h_0 as a function of gravitational-wave frequency in the ideal-MHD limit (open diamonds), calculated from ϵ_{MHD} , along with the detection thresholds for Initial and Advanced LIGO (dashed and dotted curves respectively), where we assume 14 days of coherent integration, a false alarm rate of 1 per cent, and a false dismissal rate of 10 per cent. For comparison, we plot h_{SD} (filled squares, where the arrows indicate that it is an upper limit). In the ideal-MHD limit, nine objects lie above the Initial LIGO threshold yet have not been detected (Abbott et al. 2007b), confirming that the ideal-MHD mountain relaxes substantially after accretion shuts off. More significantly, for all nine objects, h_{SD} lies below the Advanced LIGO noise curve, although PSR J0437–4715 is close. Next-generation (e.g. subterranean) interferometers will significantly lower the detection threshold, to the point where future gravitational-wave observations will constrain η_{min} more tightly than spin-down data (which are likely to be dominated by the electromagnetic torque).

4. Accreting millisecond pulsars

For AMSPs, we can derive a limit on the electrical resistivity by assuming that all objects are in spin equilibrium, such that the gravitational radiation reaction torque exactly balances the accretion torque (Bildsten 1998). Watts & Krishnan (2009) cautioned that spin balance may not hold on short time-scales. However, even if the torques do not balance

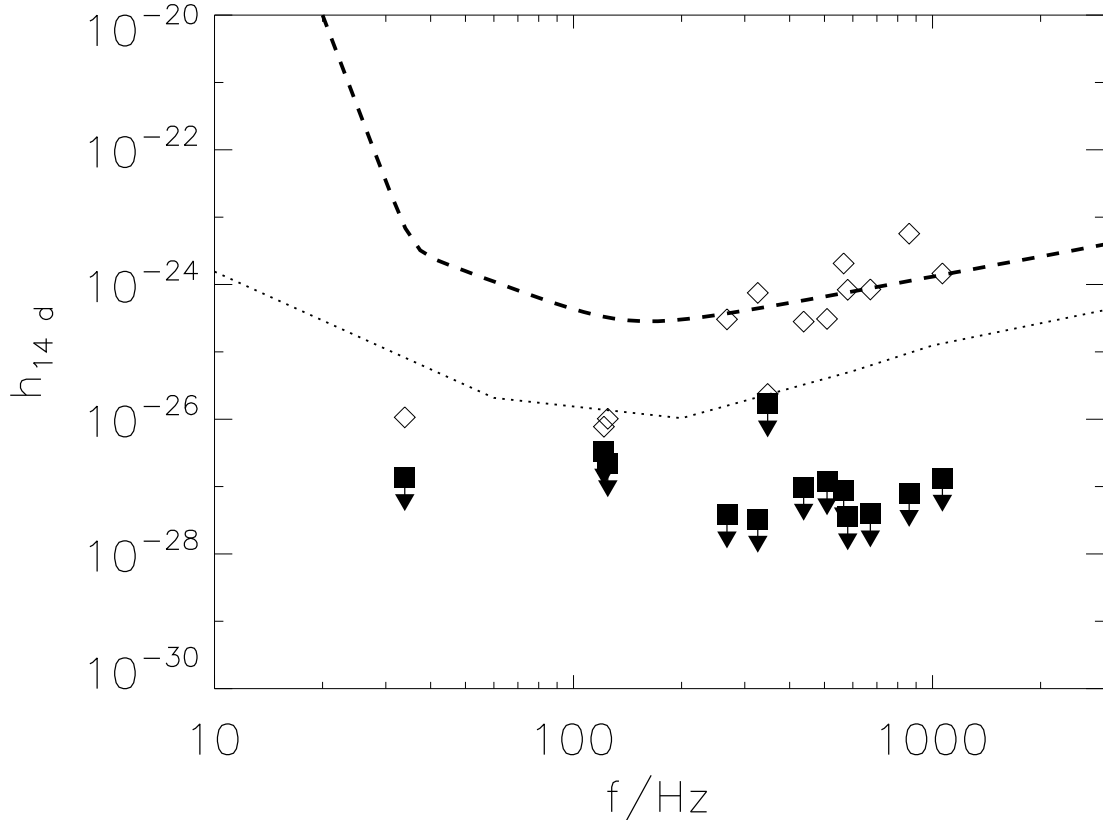


Fig. 2.— Expected gravitational wave strain h_0 in the ideal-MHD limit for the objects from van den Heuvel & Bitzaraki (1995) (open diamonds) and the spin-down lower limit h_{SD} from Eq. (5) (filled squares). We also plot the detection threshold, assuming 14 days of coherent integration, a false alarm rate of 1 per cent, and a false dismissal rate of 10 per cent, for Initial LIGO (dashed) and Advanced LIGO (dotted). Note that, although ϵ saturates for all BRMSPs ($M_a \gg M_c$), the expected gravitational wave strain depends on the distance ($h_0 \propto D^{-1}$) and is therefore different for individual objects.

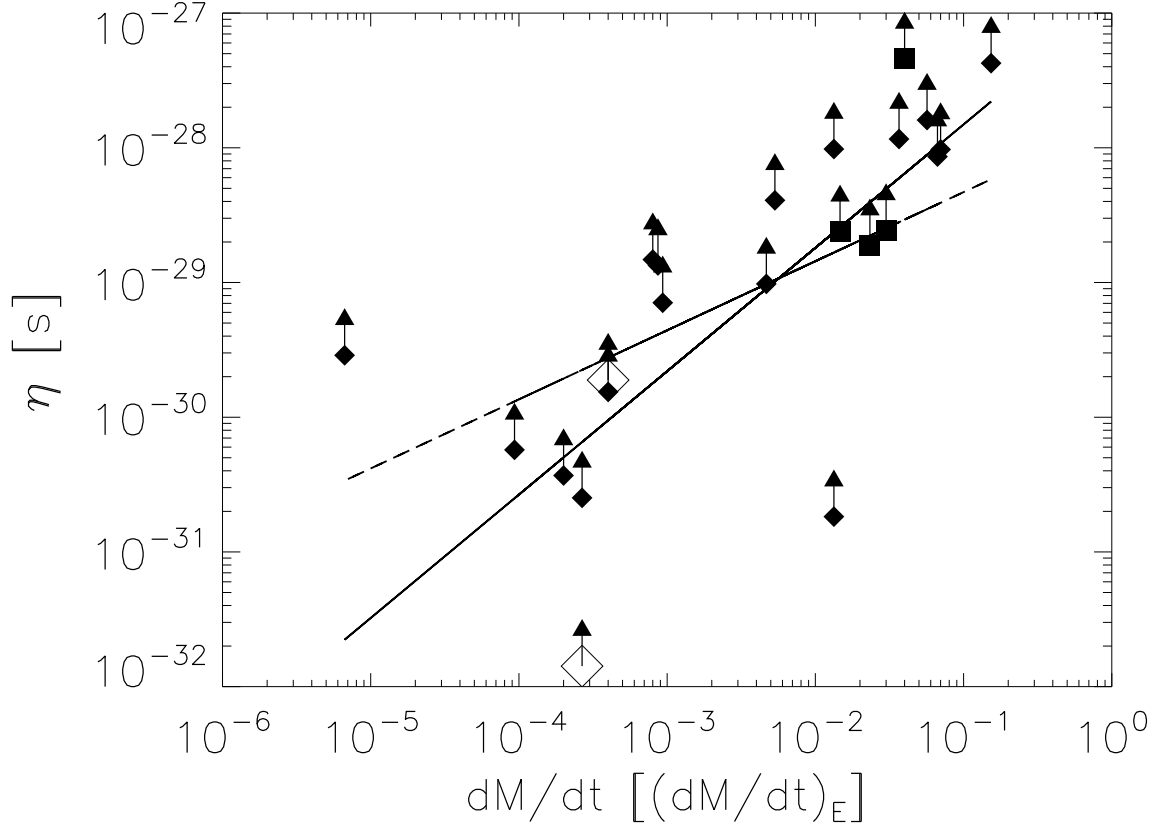


Fig. 3.— Electrical resistivity η (in s), inferred from the stalling frequency of AMSPs, plotted as a function of accretion rate \dot{M}_a (in units of the Eddington rate \dot{M}_E), inferred from the X-ray flux F_X . Lower limits on η for 17 objects from Galloway (2008) are shown as filled squares (persistent sources) and filled diamonds (transient sources). The open diamonds are lower limits inferred by the BRMSP method in §3.1 from the observed spin down between outbursts of XTE J0292–314 and SAX J1808.4–3658. The solid (dashed) line represents a power-law fit to the persistent (transient) objects.

instantaneously, it is enough for the present application that they balance on average over the long term.

Torque balance implies an indirect upper limit on the gravitational wave strain as a function of X-ray flux F_X and spin frequency,

$$\frac{h_0}{4 \times 10^{-27}} \leq \left(\frac{F_X}{10^{-8} \text{ erg s}^{-1} \text{ cm}^{-2}} \right)^{1/2} \left(\frac{f_*}{300 \text{ Hz}} \right)^{-1/2}, \quad (7)$$

or, equivalently, on the gravitational mass ellipticity,

$$\frac{\epsilon}{2 \times 10^{-7}} \leq \left(\frac{F_X}{10^{-8} \text{ erg s}^{-1} \text{ cm}^{-2}} \right)^{1/2} \left(\frac{D}{1 \text{ kpc}} \right) \left(\frac{f_*}{300 \text{ Hz}} \right)^{-5/2}, \quad (8)$$

if the star is located at a distance D . When interpreting Eq. (8) as an upper limit, it is important to keep two things in mind. (i) The X-ray emission is generally anisotropic. (ii) The accretion torque includes a magnetic component, whose lever arm, the Alfvén radius, can extend several stellar radii (Melatos & Owen 2009) [cf. Bildsten (1998)].

We are now in a position to compare the resistively relaxed quadrupole given by Eqs. (1) and (3) to the observational upper limit (8) and thus obtain a lower bound on η . Galloway (2008) tabulated D and F_X for 17 AMSPs. The key properties of these objects are listed in Table 2. Four of the objects are persistent X-ray sources; the remainder are transient, with a range of outburst and recurrence times. Burst sources are marked by an asterisk. We compute η_{\min} for these objects from Eqs. (1), (3), and (8), and plot it against \dot{M}_a in Fig. 3, where we assume that all mechanical energy of the infalling matter is converted into X-ray luminosity, viz. $F_X \approx (GM\dot{M}_a/R_*)/4\pi D^2$. A power law is a reasonable fit to the data. We find $\eta_{\min} = 10^{-26.9 \pm 0.5} (\dot{M}_a/\dot{M}_E)^{0.9 \pm 0.2}$ for the persistent objects (solid curve, fitted to the filled squares) and $\eta_{\min} = 10^{-28 \pm 4} (\dot{M}_a/\dot{M}_E)^{0.5 \pm 0.2}$ for the transient objects (dashed curve, fitted to the filled diamonds).

Two AMSPs are observed to spin down secularly between outbursts. Galloway et al. (2002) reported $\dot{f}_* = (-9.2 \pm 0.4) \times 10^{-14} \text{ Hz s}^{-1}$ in XTE J0929–314, while Hartman et al.

(2008), who followed the spin evolution of SAX J1808.4–3658 over seven years and four transient outbursts, measured $\dot{f}_* = -(5.6 \pm 2.0) \times 10^{-16} \text{ Hz s}^{-1}$. If we conservatively attribute the spin down to gravitational wave emission alone, we can obtain an independent upper limit on ϵ (and hence η_{\min}) by the BRMSP method in §3.1. For comparison, we include these lower bounds as open diamonds in Fig. 3. For XTE J0292–314, the spin-down limit falls two orders of magnitude short of the limit provided by torque balance. However, in the case of SAX J1808.4–3658, spin down during quiescence provides a slightly more stringent limit than torque balance.

5. Resistivity versus temperature

In this section, we compare the observational limits derived above with theoretical estimates for the crustal resistivity. As η is sensitive to the temperature T , which is different in BRMSPs and AMSPs, the comparison covers two decades of temperature and hence a range of scattering mechanisms.

The thermal relaxation time of a neutron star ($\sim 10^4 \text{ yr}$) is typically shorter than the accretion time-scale ($\sim 10^6 \text{ yr}$). Hence, the star is in thermal equilibrium during its X-ray lifetime (Yakovlev & Pethick 2004), with its internal temperature set by \dot{M}_a . Once accretion stops, and a BRMSP forms, the crust cools through a combination of neutrino (e.g. via direct Urca processes) and photon cooling. Competing mechanisms, such as viscous dissipation of rotational energy (Page 1998; Yakovlev et al. 1999), magnetic field dissipation (Haensel et al. 1990; Yakovlev et al. 1999; Miralles et al. 1998) and rotochemical heating (Reisenegger 1995; Cheng & Dai 1996; Reisenegger 1997; Iida & Sato 1997) act to reheat the crust. In this paper, for definiteness, we assume that reheating occurs mainly rotochemically: the rate of reactions restoring chemical equilibrium is slower than the rate of change of particle concentrations during spin down (as the centrifugal force diminishes),

Object	D	f_*	\dot{M}_a
	[kpc]	[Hz]	[$10^{-11} M_\odot \text{yr}^{-1}$]
<i>Persistent sources:</i>			
4U 1916–05*	8.9	270	22
4U 1702–429*	5.5	329	35
4U 1728–34*	5.2	363	45
<i>Transient sources:</i>			
MXB 1658–298*	12	567	60
Aql X–1	5.0	550	110
XTE J1814–338	8.0	314	1.4
4U 1608–52*	4.1	620	100
XTE J0929–314	4.0	185	0.40
Swift J1756.9–2508	8.0	182	0.14
XTE J1807–294	5.0	191	0.30
GRS 1741.9–2853*	8.0	589	0.010
XTE J1751–305	8.0	435	1.2
IGR 00291+5934	5.0	599	1.3
4U 1636–536	6.0	581	55
HETE J1900.1–2455	5.0	377	7.0
SAX J1808.4–3658	3.4	401	0.60
SAX J1748.9–2021	8.1	442	8.0
EXO 0748–676*	7.5	45.0	20
SAX J1750.8–2900*	6.8	601	20
A 1744–361*	9.0	530	230
KS 1731–26*	7.2	524	85

Table 2: Known accreting millisecond rotators [adapted from Galloway (2008) and Watts et al. (2008)]. Type I burst oscillation sources are marked with an asterisk.

so that the star is permanently out of chemical equilibrium and generates heat. If the spin-down timescale exceeds other time-scales, the temperature depends only on the current spin-down parameters, with (Fernández & Reisenegger 2005)

$$\frac{T}{T_0} = \left(\frac{|\dot{f}_*|}{10^{-16} \text{ Hz s}^{-1}} \right)^{2/7} \left(\frac{f_*}{100 \text{ Hz}} \right)^{2/7}, \quad (9)$$

and $2.8 \leq T_0/10^4 \text{ K} \leq 4.2$. The range in T_0 encompasses two realistic equations of state for the crust (Haensel & Pichon 1994; Pethick et al. 1995; Akmal et al. 1998), five equations of state for the core (Prakash et al. 1988), and a non-interacting Fermi-gas model for the whole star (Shapiro & Teukolsky 1983); see Fernández & Reisenegger (2005) for details. Below, we use Eq. (9) to compute T for BRMSPs.

No simple T - \dot{M}_a relation is available for accreting neutron stars. For the purpose of this paper, we are sensitive to η at the base of the mountain, where the bulk of the accreted matter is confined. The base is located $\sim 0.1 - 1$ km below the surface for $M_a \approx 0.1M_\odot$, where we assume that the equation of state in the crust can be modelled using a Skyrme-type effective nucleon-nucleon interaction (Douchin & Haensel 2001). An accurate treatment of the sinking problem is presented elsewhere (Wette et al. 2009). The temperature profile of the accretion column, and hence T at the mountain base, is set by nuclear heat sources inside the star, the composition of the infalling matter, and the local \dot{M}_a . It is not directly observable.

We consider two scenarios. (i) For transient sources, the temperature in the outer crust is set by a balance between deep-crustal heating during outbursts and subsequent neutrino cooling (Brown et al. 1998). The core temperature attains a steady state after $\sim 10^4$ yr (Colpi et al. 2000) and the time-averaged X-ray flux $\langle F_{\text{acc}} \rangle \approx 0.2 \langle \dot{M}_a \rangle c^2 / (4\pi D^2)$ can be related to the quiescent flux by $F_q \approx \langle F_{\text{acc}} \rangle / 135$, where we assume an accretion efficiency of 20% (Rutledge et al. 2002). We estimate the temperature by applying Fick’s law, assuming an average thermal conductivity of $\kappa \sim 10^{18} \text{ erg s}^{-1} \text{ cm}^{-1} \text{ K}^{-1}$ (Haensel & Zdunik 1990)

and a thermal length scale of $l \sim 1$ km. This procedure is only applicable if the duration of the outbursts is shorter than the thermal diffusion time of the crust, which is not always true. For example, AMSP KS 1731–260 accretes actively for $\gtrsim 13$ yr (Rutledge et al. 2002; Brown & Cumming 2009).

We note that, according to the Wiedemann-Franz law, the thermal conductivity κ and the electrical conductivity σ are related through $\kappa/\sigma = \pi^2/3(k_B/e)^2T$ at a temperature T , where e denotes the electron charge in cgs units. This agrees well with the theoretical values for σ (dashed lines in Fig. 4) under the assumption that $\kappa \sim 10^{18}$ erg s⁻¹ cm⁻¹ K⁻¹.

(ii) For persistent sources, most of the heat released by thermonuclear burning is immediately radiated outward and the interior thermal balance is dominated by pycnonuclear reactions in the deep crust. Thus, the temperature in the photosphere is set by the accretion energy flux ($\sim GM\dot{M}/r$) and gradually increases with depth by a factor of 20 – 40 to reach $(8 - 70) \times 10^8$ K at ~ 1 km (for local accretion rates per unit area in the range $5 \leq \dot{m}/\dot{m}_{\text{Edd}} \leq 40$) (Brown & Bildsten 1998). In order to place a lower bound on T (and hence a lower limit on η), we adopt two independent approaches. First, we assume that the observed X-ray flux is thermal and emitted by a polar cap with area ~ 1 km². We then apply the Stefan-Boltzmann blackbody formula, neglecting free-free corrections (Zavlin et al. 1996). The results are verified by comparing with X-ray spectral models in several objects, e.g. for IGR J00291+5934 (Falanga et al. 2005). Second, we follow a procedure similar to the transient sources by assuming that the temperature gradient is balanced by the quiescent flux (which is not observed directly but is less than the observed flux) and again apply Fick’s law.

We combine the above T estimates with the observational η limits in Fig. 4, which displays η_{min} (in s) as a function of T (in K). For BRMSPs, our fit for η_{min} as a function of τ_{SD} in Fig. 1, and the T - τ_{SD} relation in Eq. (9), convert into a resistivity-temperature

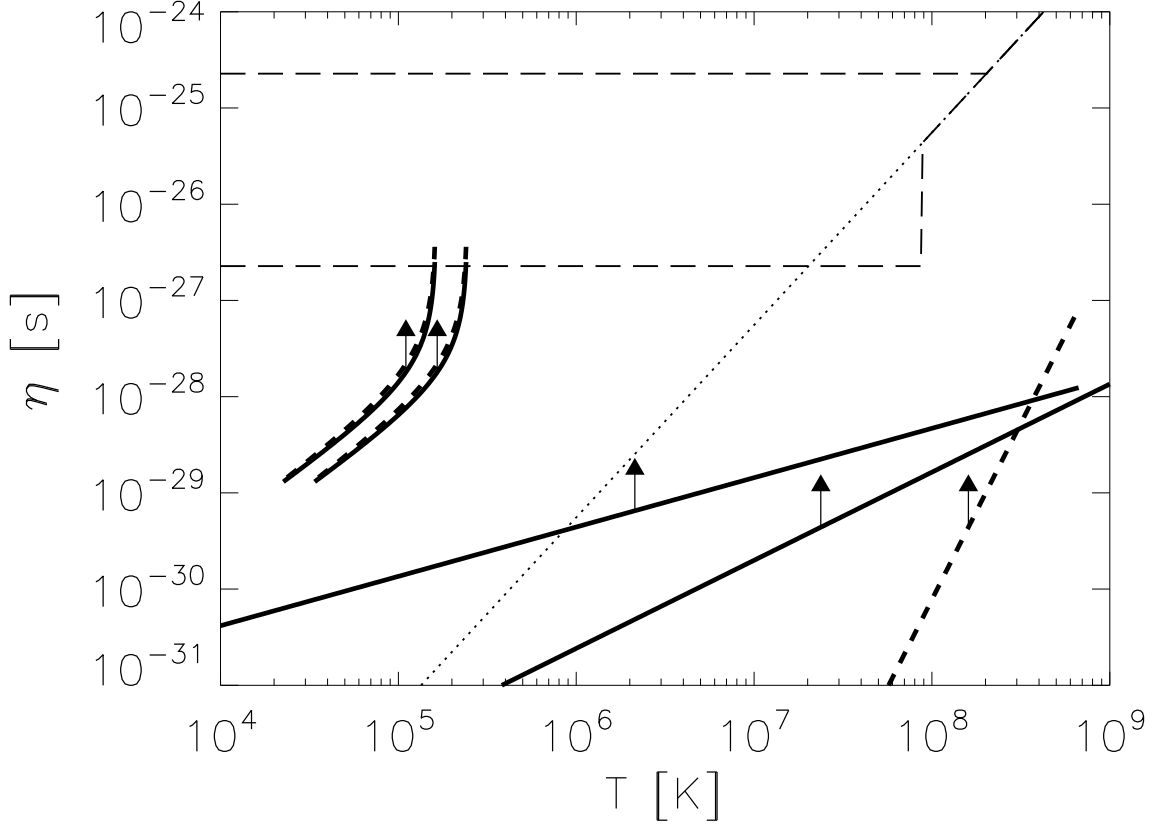


Fig. 4.— Resistivity η (in s) as a function of temperature T (in K). We show the theoretical estimates for combined electron-impurity and electron-phonon scattering as solid curves (upper curve: impurity concentration $Q = 10$, lower curve: $Q = 0.1$) and electron-phonon scattering alone (dotted curve). Lower limits $\eta_{\min}(T)$ for BRMSPs at the lower (higher) end of the range are given by the range of rotochemical equations of state [Eq. (9)]. These limits are shown as upper (lower) thick curves at the left side of the plot. The dashed curves assume that the electromagnetic torque exceeds the gravitational-wave torque by a factor of four. $\eta_{\min}(T)$ for AMSPs are displayed as thick curves at the right side of the plot. We distinguish between transient (left diagonal line) and persistent (right solid and dashed diagonal lines) accretors. For the latter, we compute the crustal temperature according to Fick’s law (solid line) and, independently, by assuming black-body emission (dashed line). The lines are all lower limits.

relation in the range $2.3 \times 10^4 \text{ K} \leq T \leq 1.6 \times 10^5 \text{ K}$. We plot $\eta_{\min}(T)$ as a pair of thick solid curves in the left half of Fig. 4; the lower and upper curves correspond to $T_0 = 4.2 \times 10^4 \text{ K}$ and $T_0 = 2.8 \times 10^4 \text{ K}$ respectively [cf. Eq. (9)]. For AMSPs, we translate $\eta_{\min}(\dot{M}_a)$ into $\eta_{\min}(T)$ as detailed above, where we distinguish between (i) persistent accretors assuming black body radiation (right-most, dashed diagonal line), persistent accretors applying Fick’s law (lower diagonal line), and transient accretors (upper diagonal line), in the range $10^{-13} \leq \dot{M}_a/M_\odot \text{ yr}^{-1} \leq 10^{-8}$ populated by the objects in Fig. 3. For comparison, we overplot the theoretical resistivity for combined electron-impurity and electron-phonon scattering for impurity concentrations $Q = 10$ and 0.1 (upper and lower dashed curves, respectively).

The electrical conductivity of the neutron star crust is caused by electron scattering off phonons and impurities (Cumming et al. 2001, 2004). For temperatures below the Umklapp temperature ($T_U \approx 10^7 \text{ K}$), electron-phonon scattering is suppressed. In rapid accretors ($\dot{M}_a \gtrsim 10^{-11} M_\odot \text{ yr}^{-1}$), phonon scattering dominates for $Q \lesssim 1$. The impurity fraction depends on the composition of the ashes produced in steady-state nuclear burning at low densities. Schatz et al. (1999) found a large variety of nuclei in the crust, with $Q \approx 100$, except in rapid accretors ($Q \sim 1$ for $\dot{M} \gtrsim 30\dot{M}_E$). Jones (2004a) noted that, if the primordial crust is completely replaced by heterogeneous accreted matter, one has $Q \gg 1$. Other authors adopt lower fractions. For example, Pons & Geppert (2007) preferred $10^{-4} \lesssim Q \lesssim 10^{-2}$ in their model for magnetic field dissipation.

6. Discussion

Fig. 4 indicates that spin-down and indirect gravitational-wave stalling limits are on the verge of challenging theoretical models of the electrical resistivity of the accreted crust in a neutron star. The limits from BRMSPs assuming rotochemical heating intersect the

$Q = 0.1$ electron-impurity curve above $T \gtrsim 10^5$ K. Hence, very young BRMSPs (upper end of the curves) tentatively exclude impurity concentrations $Q \lesssim 0.1$ and will place even stricter limits on Q as younger objects are found.

Brown & Cumming (2009) constrained Q by fitting theoretical cooling models to observed post-outburst light curves of KS 1731–260 and MXB 1659–29. These authors found $Q \sim 1$, and certainly $Q \ll 10$, in close agreement with Shternin et al. (2007). Molecular dynamics simulations confirm this result (Horowitz et al. 2008; Horowitz & Kadau 2009), revealing a phase-separated regular crystal, with low- Q regions embedded in a high- Q phase. One interesting possibility is that the solid phase of the crust in isolated neutron stars is heterogenous with respect to the nuclear charge (Jones 2004b), lowering the resistivity by four orders of magnitude to $\eta \approx 10^{-24}$ s. Recent observations of cooling curves after extended outbursts (Wijnands 2004; Cackett et al. 2006) suggest a high *thermal* conductivity of the crust, typical of a regular crystal (Rutledge et al. 2002; Shternin et al. 2007).

Future gravitational wave experiments will tighten the above limits. Advanced LIGO, for example, offers a narrowband configuration, which lowers the instrumental noise by two orders of magnitude (Abbott 2007a). The main challenge to searches is posed by parameter uncertainties (Watts et al. 2008). Here, simultaneous electromagnetic observations will prove beneficial, reducing the number of search templates and the computational effort. In any case, this paper illustrates one of the ways in which even gravitational-wave nondetections yield important independent information about the constitutive properties of neutron stars.

Several shortcomings in the theoretical modelling of magnetic mountains still need to be addressed, most notably sinking of the mountain into the crust (Wette et al. 2009), and a realistic equation of state which includes nuclear reactions. In addition, in the

context of this article, it is important to ultimately include the Hall effect. While it is not dissipative, the Hall effect transfers magnetic energy from large to small scales through a Hall cascade (Goldreich & Reisenegger 1992). The small-scale magnetic structures subsequently decay on the Ohmic timescale. The Hall timescale, t_{Hall} , has been computed for neutron star crusts by Cumming et al. (2004), who found $10^3 \lesssim t_{\text{Hall}}/\text{yr} \lesssim 10^7$, well below the typical X-ray lifetime of an LMXB. This result, however, is only valid as long as the impurity factor Q is low. For higher $Q \gtrsim 1$, Ohmic dissipation always dominates Hall dissipation (Cumming et al. 2004). Furthermore, a subsurface toroidal magnetic field can create small-scale poloidal field structures through a Hall-drift induced instability, where a background shear in the electron velocity drives the growth of long-wavelength modes (Cumming et al. 2004; Geppert et al. 2003; Rheinhardt & Geppert 2002). The consequences of this instability for the magnetic field evolution in neutron stars are still unclear; perturbations to the crustal field are effectively reflected by the solid/fluid interface and might be trapped in the lower crust layers (Cumming et al. 2004).

In this paper, the theoretical ϵ is intentionally calculated differently for BRMSPs and AMSPs. On the face of it, this seems unnecessary, given that BRMSPs evolve from AMSPs. But we are forced to take this approach because we do not know the historic \dot{M}_a for any specific BRMSP. Hence, we cannot apply Eq. (1) to get ϵ_{MHD} , while Eq. (2) does not apply in the context of ongoing accretion. On the plus side, however, the effect of Ohmic diffusion during ongoing accretion has not been studied properly in two and three dimensions, as Cumming et al. (2001) pointed out. It is therefore an advantage to have two independent calculations for the two classes of objects, pending further studies.

Finally, if the magnetic mountain picture of field evolution is accurate, then the spin-down limits in §3.1 can be combined with magnetic moment data for BRMSPs to test the self-consistency of the argument in this paper. For example, if the buried magnetic

field is anchored deep in the core, it resurrects as the mountain relaxes resistively, tending towards its natal value over many τ_d . This can lead to an inconsistency if $\epsilon_{SD}/\epsilon_{MHD}$ is too small, for then the resurrected magnetic moment may exceed the value observed. Unfortunately, the above test cannot be applied (yet) with confidence, because it rests heavily on the assumption that the magnetic field is anchored in the core. If, by contrast, the source currents are confined to the crust, minimal field resurrection occurs; both ϵ and the magnetic moment decay resistively, and no useful constraint emerges. The question of where the field is anchored, crust or core, is hotly debated and remains one of the main obstacles in understanding magnetic field evolution in accreting neutron stars (Konar & Bhattacharya 1997; Ruderman et al. 1998; Pons et al. 2009).

M.V. acknowledges the support of The University of Melbourne through a David Hay Postgraduate Writing-Up Award.

REFERENCES

- Abbott, B., et al. 2007a, *Phys. Rev. D*, 76, 082003
- . 2007b, *Phys. Rev. D*, 76, 042001
- . 2008, *ApJ*, 683, L45
- Abbott, B. e. 2007a, Advanced LIGO reference design, Tech. rep., online Document:
<http://www.ligo.caltech.edu/docs/M/M060056-08/M060056-08.pdf>
- . 2007b, *Phys. Rev. D*, 76, 082001
- Akmal, A., Pandharipande, V. R., & Ravenhall, D. G. 1998, *Phys. Rev. C*, 58, 1804
- Alpar, M. A. 2008, in American Institute of Physics Conference Series, Vol. 1068, American Institute of Physics Conference Series, ed. R. Wijnands, D. Altamirano, P. Soleri, N. Degenaar, N. Rea, P. Casella, A. Patruno, & M. Linares, 3–8
- Arzoumanian, Z., Chernoff, D. F., & Cordes, J. M. 2002, *ApJ*, 568, 289
- Baiko, D. A., & Yakovlev, D. G. 1996, *Astronomy Letters*, 22, 708
- Bildsten, L. 1998, *ApJ*, 501, L89+
- Bonazzola, S., & Gourgoulhon, E. 1996, *A&A*, 312, 675
- Brown, E. F., & Bildsten, L. 1998, *ApJ*, 496, 915
- Brown, E. F., Bildsten, L., & Rutledge, R. E. 1998, *ApJ*, 504, L95+
- Brown, E. F., & Cumming, A. 2009, *ApJ*, 698, 1020
- Cackett, E. M., Wijnands, R., Linares, M., Miller, J. M., Homan, J., & Lewin, W. H. G. 2006, *MNRAS*, 372, 479

- Cheng, K. S., & Dai, Z. G. 1996, *ApJ*, 468, 819
- Chung, C. T. Y., Galloway, D. K., & Melatos, A. 2008, *MNRAS*, 391, 254
- Colpi, M., Geppert, U., & Page, D. 2000, *ApJ*, 529, L29
- Cumming, A., Arras, P., & Zweibel, E. 2004, *ApJ*, 609, 999
- Cumming, A., Zweibel, E., & Bildsten, L. 2001, *ApJ*, 557, 958
- Cutler, C. 2002, *Phys. Rev. D*, 66, 084025
- Douchin, F., & Haensel, P. 2001, *A&A*, 380, 151
- Falanga, M., Kuiper, L., Poutanen, J., Bonning, E. W., Hermsen, W., di Salvo, T., Goldoni, P., Goldwurm, A., Shaw, S. E., & Stella, L. 2005, *A&A*, 444, 15
- Faucher-Giguère, C.-A., & Kaspi, V. M. 2006, *ApJ*, 643, 332
- Fernández, R., & Reisenegger, A. 2005, *ApJ*, 625, 291
- Galloway, D. 2008, in *American Institute of Physics Conference Series*, Vol. 983, 40 Years of Pulsars: Millisecond Pulsars, Magnetars and More, 510–518
- Galloway, D. K., Chakrabarty, D., Morgan, E. H., & Remillard, R. A. 2002, *ApJ*, 576, L137
- Geppert, U., Rheinhardt, M., & Gil, J. 2003, *A&A*, 412, L33
- Goldreich, P., & Reisenegger, A. 1992, *ApJ*, 395, 250
- Haensel, P., & Pichon, B. 1994, *A&A*, 283, 313
- Haensel, P., Urpin, V. A., & Iakovlev, D. G. 1990, *A&A*, 229, 133
- Haensel, P., & Zdunik, J. 1990, *Astron. Astrophys.*, 229, 117

- Hameury, J. M., Bonazzola, S., Heyvaerts, J., & Lasota, J. P. 1983, *A&A*, 128, 369
- Hartman, J. M., Patruno, A., Chakrabarty, D., Kaplan, D. L., Markwardt, C. B., Morgan, E. H., Ray, P. S., van der Klis, M., & Wijnands, R. 2008, *ApJ*, 675, 1468
- Hartman, J. W., Bhattacharya, D., Wijers, R., & Verbunt, F. 1997, *A&A*, 322, 477
- Haskell, B., Andersson, N., Jones, D. I., & Samuelsson, L. 2007, *Physical Review Letters*, 99, 231101
- Heyl, J. S. 2002, *ApJ*, 574, L57
- Hobbs, G., Manchester, R., Teoh, A., & Hobbs, M. 2004, in *IAU Symposium*, 139–+
- Horowitz, C. J., Caballero, O. L., & Berry, D. K. 2008, preprint (astro-ph/0804.4409), 804
- Horowitz, C. J., & Kadau, K. 2009, preprint (astro-ph/0904.1986)
- Iida, K., & Sato, K. 1997, *ApJ*, 477, 294
- Itoh, N., & Kohyama, Y. 1993, *ApJ*, 404, 268
- Jaranowski, P., Królak, A., & Schutz, B. F. 1998, *Phys. Rev. D*, 58, 063001
- Jones, P. B. 2004a, *Physical Review Letters*, 93, 221101
- . 2004b, *MNRAS*, 351, 956
- Konar, S., & Bhattacharya, D. 1997, *MNRAS*, 284, 311
- Litwin, C., Brown, E. F., & Rosner, R. 2001, *ApJ*, 553, 788
- Melatos, A., & Owen, B. 2009, in preparation
- Melatos, A., & Payne, D. J. B. 2005, *ApJ*, 623, 1044

- Miralles, J. A., Urpin, V., & Konenkov, D. 1998, *ApJ*, 503, 368
- Owen, B. J. 2009, preprint (astro-ph/0904.4848)
- Page, D. 1998, in *NATO ASIC Proc. 515: The Many Faces of Neutron Stars.*, ed. R. Buccheri, J. van Paradijs, & A. Alpar, 539–+
- Payne, D. J. B., & Melatos, A. 2004, *MNRAS*, 351, 569
- . 2006, *ApJ*, 641, 471
- Pethick, C. J., Ravenhall, D. G., & Lorenz, C. P. 1995, *Nuclear Physics A*, 584, 675
- Pons, J. A., & Geppert, U. 2007, *A&A*, 470, 303
- Pons, J. A., Miralles, J. A., & Geppert, U. 2009, *A&A*, 496, 207
- Prakash, M., Lattimer, J. M., & Ainsworth, T. L. 1988, *Physical Review Letters*, 61, 2518
- Priymak, M., & Melatos, A. 2009, in preparation
- Reisenegger, A. 1995, *ApJ*, 442, 749
- . 1997, *ApJ*, 485, 313
- Rheinhardt, M., & Geppert, U. 2002, *Physical Review Letters*, 88, 101103
- Ruderman, M., Zhu, T., & Chen, K. 1998, *ApJ*, 492, 267
- Rutledge, R. E., Bildsten, L., Brown, E. F., Pavlov, G. G., Zavlin, V. E., & Ushomirsky, G. 2002, *ApJ*, 580, 413
- Schatz, H., Bildsten, L., Cumming, A., & Wiescher, M. 1999, *ApJ*, 524, 1014

- Shapiro, S. L., & Teukolsky, S. A. 1983, Black holes, white dwarfs, and neutron stars: The physics of compact objects (Research supported by the National Science Foundation. New York, Wiley-Interscience, 1983, 663 p.)
- Shternin, P. S., Yakovlev, D. G., Haensel, P., & Potekhin, A. Y. 2007, MNRAS, 382, L43
- Ushomirsky, G., Cutler, C., & Bildsten, L. 2000, MNRAS, 319, 902
- Van Den Broeck, C. 2005, Classical and Quantum Gravity, 22, 1825
- van den Heuvel, E. P. J., & Bitzaraki, O. 1995, A&A, 297, L41+
- van Eysden, C. A., & Melatos, A. 2008, Classical and Quantum Gravity, 25, 225020
- Vigelius, M., & Melatos, A. 2008, MNRAS, 386, 1294
- . 2009a, MNRAS, 395, 1972
- . 2009b, MNRAS, 395, 1985
- Watts, A. L., & Krishnan, B. 2009, Advances in Space Research, 43, 1049
- Watts, A. L., Krishnan, B., Bildsten, L., & Schutz, B. F. 2008, MNRAS, 389, 839
- Wette, K., Vigelius, M., & Melatos, A. 2009, in preparation
- Wette, K., et al. 2008, Classical and Quantum Gravity, 25, 235011
- Wijers, R. A. M. J. 1997, MNRAS, 287, 607
- Wijnands, R. 2004, in Chandra Proposal, 1673–+
- Wijnands, R., & van der Klis, M. 1998, Nature, 394, 344
- Yakovlev, D. G., Levenfish, K. P., & Shiblanov, Y. A. 1999, Soviet Physics Uspekhi, 42, 737

Yakovlev, D. G., & Pethick, C. J. 2004, *ARA&A*, 42, 169

Zavlin, V. E., Pavlov, G. G., & Shibano, Y. A. 1996, *A&A*, 315, 141

Zimmermann, M., & Szedenits, Jr., E. 1979, *Phys. Rev. D*, 20, 351